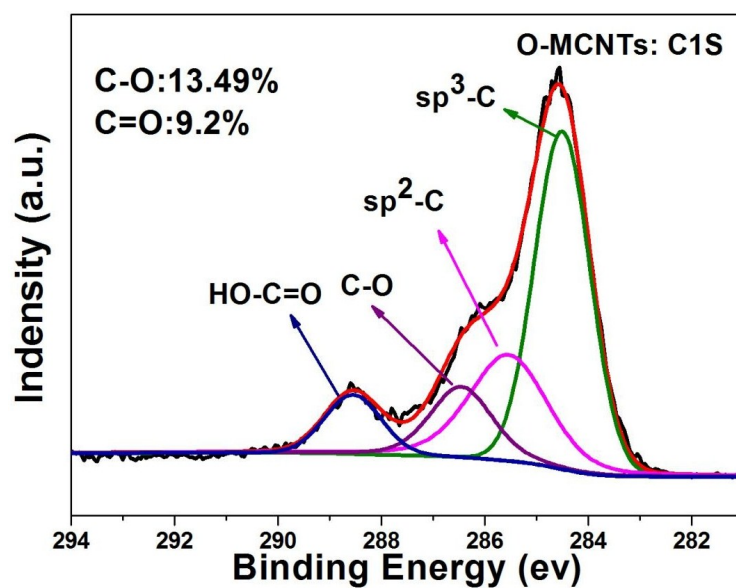


## Supporting Information

### **A Novel Synthesis of Carbon Nanotubes Directly from Indecomposable Solid Carbon Source for Electrochemical Applications**

*Zhi Zhang<sup>1</sup>, Shichun Mu<sup>2</sup>, Bowei Zhang<sup>3</sup>, Lu Tao<sup>1</sup>, Shifei Huang<sup>1</sup>, Yizhong Huang<sup>3</sup> and  
Faming Gao<sup>1</sup>, Yufeng Zhao<sup>1</sup>\**



**Figure S1.** C1S XPS spectra of O-MCNTs

As shown in **Figure S1**, the C1s core-level XPS spectrum of O-MCNTs is curve-fitted into four peaks, corresponding to C-C (SP<sup>3</sup>-C, 284.48 eV) 51.47%, C=C (SP<sup>2</sup>-C, 285.28 eV) 25.84%, C-O (hydroxyl, 286.48 eV), HO-C=O (288.7 eV), respectively<sup>1</sup>.

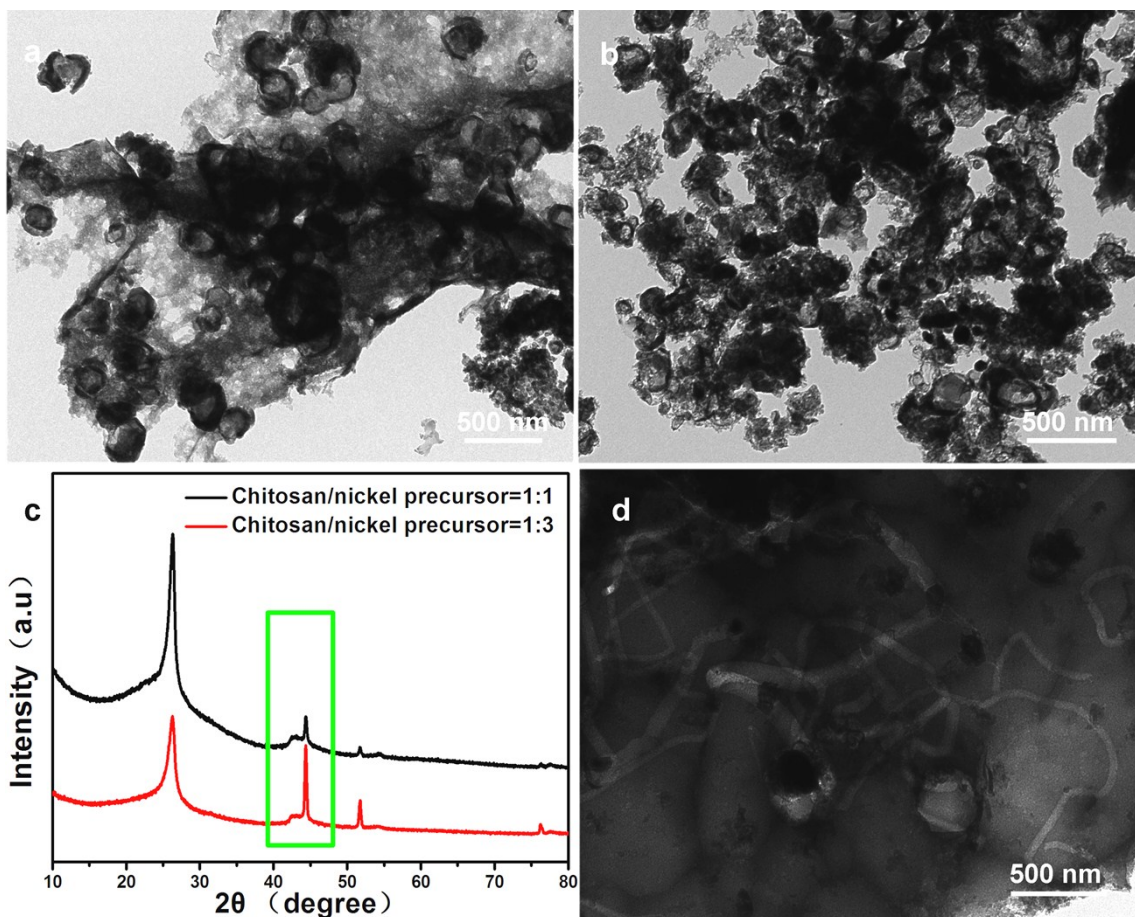


**Figure S2.** TEM images of intermediate product produced at 800 °C with different amount of Ni precursor added to the chitosan: (a)  $W_{\text{chitosan}}/W_{\text{nickel precursor}}=1:1$ , (b)  $W_{\text{chitosan}}/W_{\text{nickel precursor}}=1:3$ ; (c) XRD pattern of intermediate products ( $W_{\text{chitosan}}/W_{\text{nickel precursor}}=1:1$  and  $1:3$ ); (d) TEM images of final product after KOH induced SVCD process ( $W_{\text{chitosan}}/W_{\text{nickel precursor}}=1:3$ ).

As comparison, chitosan powder was applied as precursor to fabricate CNTs through the same procedure. **Figure S2a** and **b** show the TEM images of the intermediate product with different amount of Ni ions added to chitosan precursor, Ni nanoparticles are imbedded into the intermediate product but the distribution is not uniform. XRD patterns prove the successful loading of Ni into the intermediated (**Figure S2c**). Notably, after catalyzed gasification reaction, some tube-like structure appear are also observed in the final product ( $W_{\text{chitosan}}/W_{\text{nickel precursor}}=1:3$ ), further demonstrating the feasibility of this proposed mechanism (**Figure S2d**). The nonuniform morphology of the as produced CNTs could be attributed to the inhomogeneous distribution of the Ni catalyst.

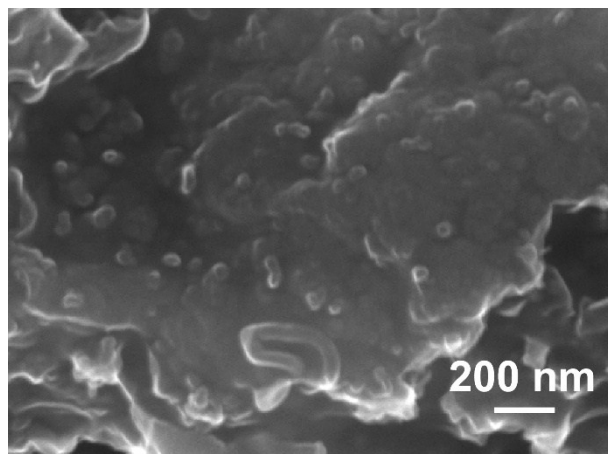


**Figure S3.** SEM images of the as-synthesized O-MCNTs at 850 °C for weight ratio  
( $W_{\text{KOH}}/W_{\text{Ni-GPCF}}=1$ ).

When  $W_{\text{KOH}}/W_{\text{Ni-GPCF}}$  equals to 1, the 3D porous structure of Ni-GPCF collapsed and no obvious tube morphology was observed (**Figure S3**).

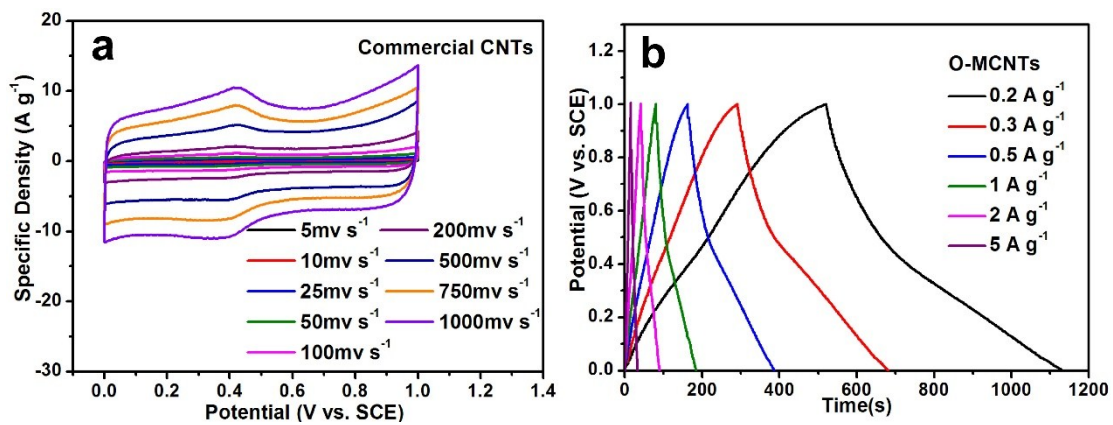


**Figure S4.** (a) CV of commercial CNTs at the scan rate from 5-1000  $mv s^{-1}$ ; (b) Galvanostatic charge/discharge curves of O-MCNTs at different current density from 0.2-5  $A g^{-1}$ ;

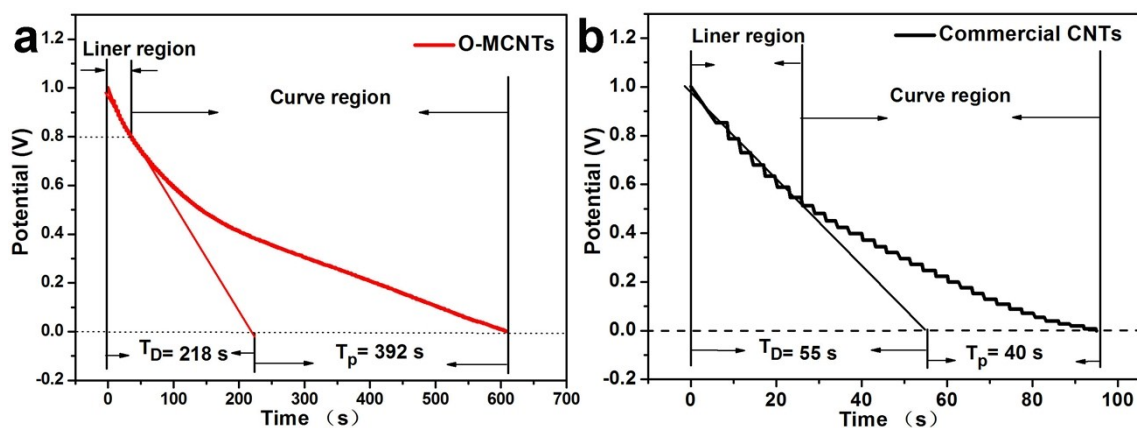


**Figure S5.** Discharge time of the pseudocapacitance parts of the O-MCNTs (a); and commercial CNTs (b) at the current density of  $0.2 \text{ A g}^{-1}$ .

As shown in **Figure S5**, the charge-discharge curves include curve section and straight linear section, corresponding to the pseudocapacitance ( $C_p$ ) and electric double layer capacitance ( $C_{EDL}$ ), respectively. The discharge time was divided into  $T_D$  (discharge time of the  $C_{EDL}$  type) and  $T_p$  (discharge time of the  $C_p$  type) by extending linear part of discharge curve to X-axis. The corresponding pseudocapacitance ( $C_p$ ) calculated from the  $T_p$  of O-MCNTs is  $78 \text{ F g}^{-1}$ , which is obviously found that the percentage of oxygen groups' contribution to the  $C_s$  is 64%. For comparison, the pseudocapacitance values of commercial CNTs was also calculated as  $8 \text{ F g}^{-1}$  (**Figure S5b**).



**Figure S6.** The photograph of the semiconductor powder resistivity apparatus. The pressure used here was 5 MPa.

The electric conductivity of the O-MCNTs and CVD-synthesized CNTs was measured with the semiconductor powder resistivity apparatus (ST-2722, Suzhou Jingge Electronic Co. Ltd., China), which is 289.4 and 447.5 S m<sup>-1</sup>, respectively. The smaller conductivity of the O-MCNTs than commercial CNTs should be attributed to the high content defects and oxygen functional groups.

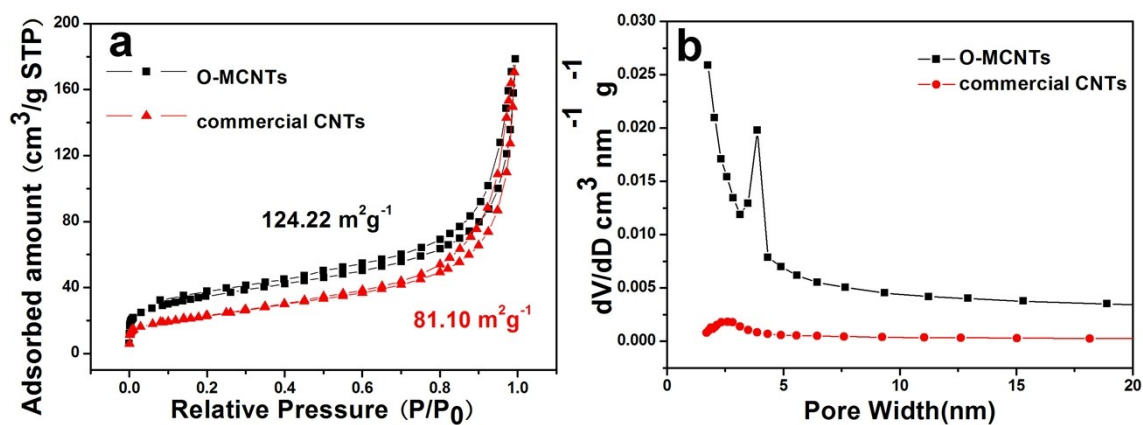


**Figure S7.** (a)  $N_2$  adsorption-desorption isotherms of O-MCNTs and commercial CVD synthesized CNTs; (b) the corresponding pore size distribution of the O-MCNTs and commercial CVD synthesized CNTs.

The  $N_2$  adsorption-desorption isotherms and the corresponding pore size distribution of O-MCNTs and commercial CVD synthesized CNTs are shown in Figure S6. The BET (Brunauer–Emmett–Teller) specific surface area and BJH (Barrett-Joyner-Halenda) average pore size are calculated to be  $124.2 \text{ m}^2 \text{ g}^{-1}$  and  $3.88 \text{ nm}$  for O-MCNTs, and  $81.10 \text{ m}^2 \text{ g}^{-1}$  and  $2.59 \text{ nm}$  for CVD synthesized CNTs (purchased from Beijing DK Nano Technology Co. Ltd., China), respectively.



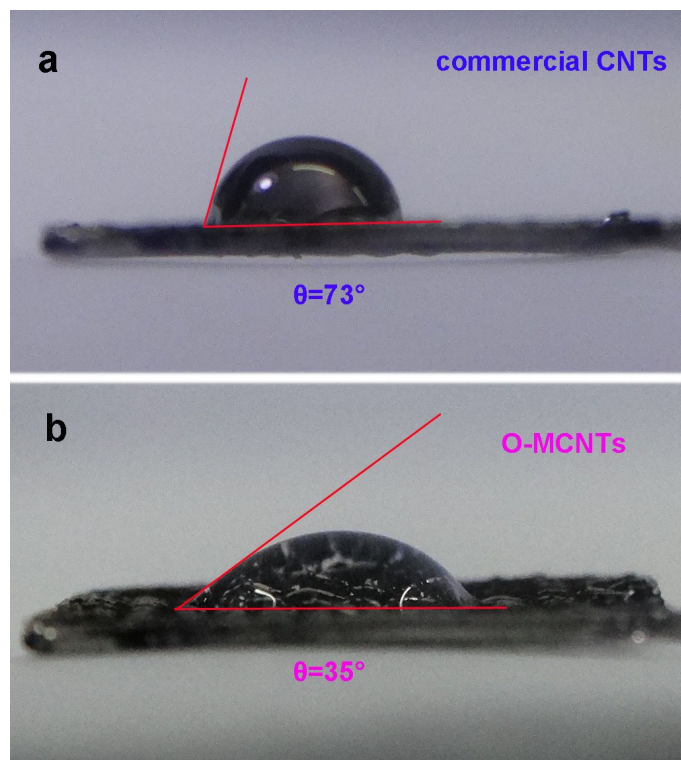


**Figure S8.** Contact angles of 1 M H<sub>2</sub>SO<sub>4</sub> droplet attached on commercial CNTs (73°) and O-MCNTs (35°) substrates.

The wettability was tested by measure the contact angles of the 1M H<sub>2</sub>SO<sub>4</sub> droplet on the Pt nets coated with same amount of O-MCNTs and CNTs, respectively (**Figure S8**). Apparently, O-MCNTs present better hydrophilic property than commercial CNTs, with a much smaller contact angle.

#### Reference

[1] L. Hao, X. L. Li, L. J. Zhi, Adv. Mater. 2013, 25, 3899-3904.